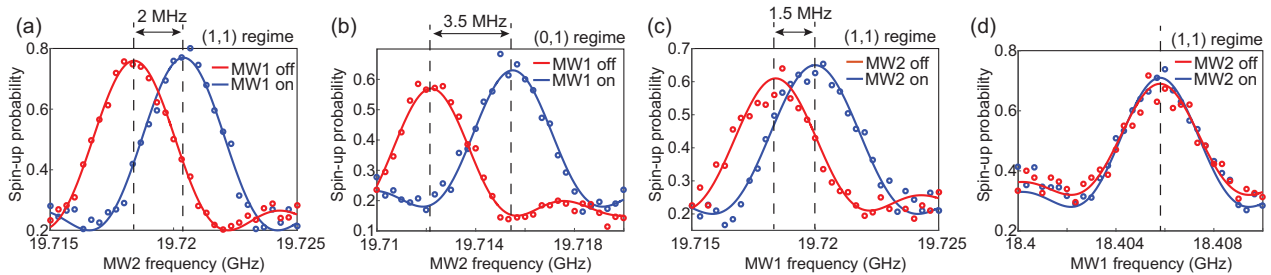## S1. FREQUENCY SHIFTS ON Q2 DUE TO OFF-RESONANT FREQUENCY PULSES

As discussed in the main manuscript, we observe a large frequency shift on Q2 while applying off-resonant microwaves (MW). Similar effects have been observed for electron spins bound to single donor atoms [1] but with a significantly smaller frequency shift and with transient behaviour occurring over $\sim 100\mu s$. In our experiment the microwave source MW1 (MW2) applies MWs to gate P3 (P4) to manipulate Q1 (Q2) as shown in Extended Data Fig. 1. Fig. S1(a) shows the resonant frequency of Q2 shifting by 2 MHz while off-resonant MWs of 18.5 GHz are applied with MW1 via P3. One possible mechanism to explain this effect is the AC stark shift, where off-resonance MW's will shift the qubit's resonance frequency (ω_L) by $\sim \omega_R^2/2(\omega_1 - \omega_L)$ away from the drive frequency, ω_1 [2]. However, this is a negligible effect and the observed frequency shift is towards the off-resonant MW frequency ruling out the AC-stark shift as a possible cause. We also performed the same experiment in the (0,1) charge regime where we observed similar behaviour (Fig. S1(b)) eliminating effects due to the coupling between the two electron spins. Fig. S1(c) shows that the resonant frequency also shifts if instead we apply off-resonant MWs using MW2 via P4 demonstrating that this effect does not depend on the gate electrode/coaxial line used to apply the MW's. Interestingly, we do not see the effect on the other qubit as shown in Fig. S1(d) where we apply off-resonant microwaves at 18.5 GHz at nearly the maximum output power ($P = 22$ dBm) of the MW2 source suggesting that the effect is due to some property of the quantum dot. The frequency shift is also measured in a Ramsey sequence where during the $\pi/2$ pulse both MW sources are on and during the wait time both MW sources are off. This indicates the frequency shift occurs faster than the Ramsey wait time (<100 ns) ruling out local heating effects which would require time to dissipate. Finally, we observe that the frequency shift is strongly dependent on the power of the off-resonance MW's as shown in Fig. S2.
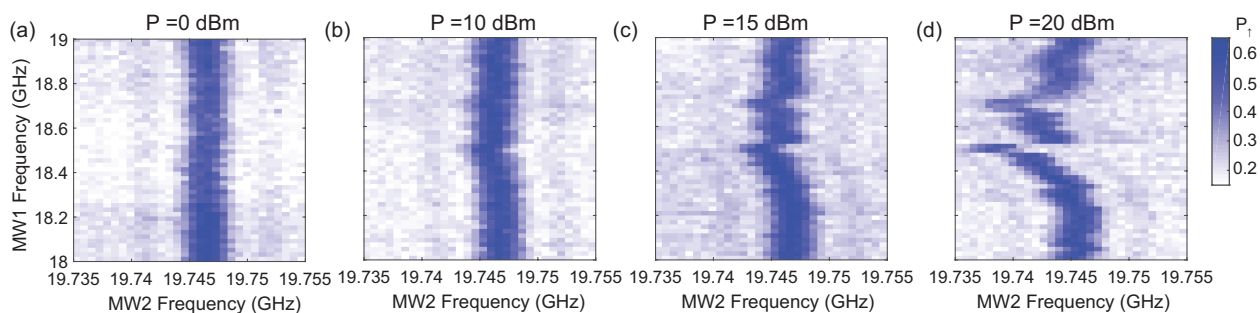

Supplementary Fig. S1. **Frequency shift on Q2 due to off-resonant microwaves signals.** (a) Spectroscopy of Q2 with MW2 while MW1 is either off (blue data) or applying off-resonant MWs (red) to plunger gate P3 with a frequency $f = 18.5$ GHz and power $P = 16$ dBm. (b) The same experiment is performed in the (0,1) charge regime where there is only one electron in the double quantum dot. (c) Spectroscopy of Q2 with MW1 while MW2 is off (blue data) or applying off-resonant MWs (red) to plunger gate P4 with a frequency $f = 18.5$ GHz and power $P = 10$ dBm. (d) Spectroscopy of Q1 with MW1 while MW2 is off (blue data) or applying off-resonant MWs (red) to plunger gate P4 with a frequency $f = 18.5$ GHz and power $P = 22$ dBm.

The dependence on the quantum dot properties and power would be compatible with the rectification of the AC signal as an explanation. An asymmetric quantum dot potential will lead to a DC displacement in response to an AC excitation on the gate. We tried to estimate this by measuring the resonance frequency of Q2 as a function of the voltage applied on plunger P3 around the position in gate-space where we perform the single-qubit gates. Over the estimated range of the AC signal, $V_{RMS} \sim 5$ mV for an output power of $P = 16$ dBm and measured attenuation of the coaxial line (~ 43 dB at 20 GHz), we observe a change in frequency of ~ 1 MHz and no measurable non-linearity in the resonance frequency. While this suggests rectification effects are small, it is difficult to get an accurate estimation on the AC signal at the sample and further work is required to rule out this possibility.
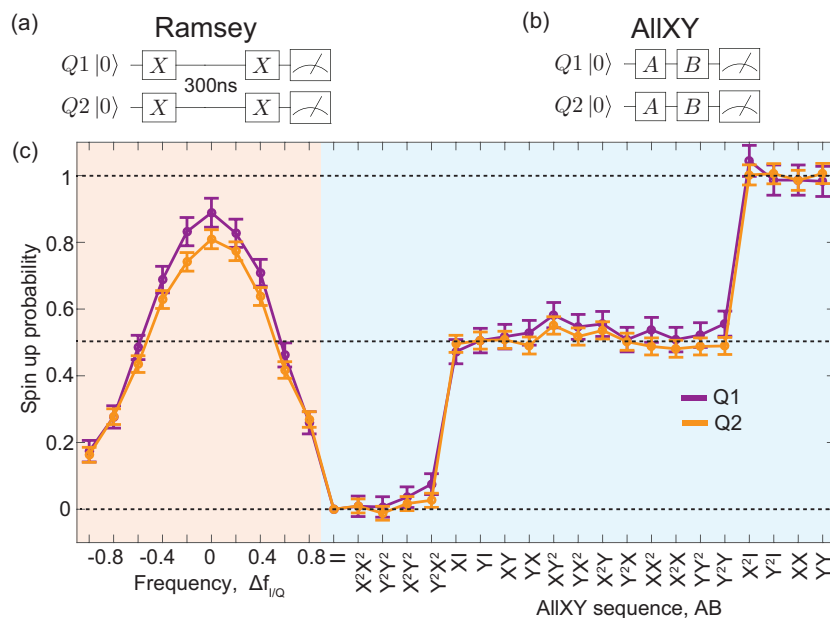
S2. CALIBRATION OF SINGLE-QUBIT GATES.

To perform accurate single-qubit gates on Q1 and Q2 we need to calibrate the following parameters of our MW pulses, (i) the frequency needed to be on resonance with Q1 and Q2, (ii) the power needed to perform a $\pi/2$ pulse on Q1 and Q2, (iii) the power needed for the 30 MHz off-resonance pulse during Q1 idle times to compensate for the Q2 frequency shift described above. The resonance frequency of Q1 (Q2) was measured using the Ramsey sequence shown

Supplementary Fig. S2. **Power dependence of the Q2 frequency shift.** Spectroscopy maps showing the resonance frequency of Q2 measured with MW2 as a function of the off-resonant MW frequency applied using MW1. These maps are measured at MW1 powers (a) 0 dBm, (b) 10 dBm, (c) 15 dBm, and (d) 20 dBm. The larger shifts in the resonance frequency most likely occur at transmission resonances where the power applied on the device is larger.

in Supplementary Fig. S3(a) and corresponds to the MW frequency that gives the maximum spin-up probability for Q1 (Q2). During the 300 ns wait time we apply the off-resonant MW pulse to Q1 to keep the resonance frequency of Q2 constant throughout the sequence. The power of the applied MW pulses was calibrated using the AllXY calibration sequence. In this sequence, two single-qubit gates, A and B where $A, B \in \{I, X, X^2, Y, Y^2\}$, are applied sequentially to the qubit as shown in Supplementary Fig. S3(b). All possible combinations of A and B are applied and the final spin-up probabilities are measured. If the gates are ideal then the different combinations give the expected final probability of either 0, 0.5, or 1. MW power and frequency errors during the single-qubit gates result in characteristic deviations from these probabilities and can be corrected. In addition, if there is an error in the applied power of the off-resonant MW pulse during the Ramsey calibration so that the resonance frequency of Q2 is not the same during the wait time and the X gates, this will show up as a frequency error in the AllXY sequence and can also be easily corrected. Supplementary Fig. S3(c) shows an example of the result of the Ramsey and AllXY sequences after all the parameters have been calibrated.

Supplementary Fig. S3. **Calibration of the single-qubits gates.** (a) Ramsey and (b) AllXY sequences used to calibrate the single-qubit gates for Q1 and Q2. (c) The measured spin-up probability of Q1 (purple data points) and Q2 (orange data points) during the Ramsey and AllXY experiments after the single-qubit gates have been calibrated. Here, errors due to readout have been removed from the spin-up probabilities. In the Ramsey experiment the MW frequency is swept around the local oscillator frequency of the MW source using I/Q modulation. In the AllXY experiment the x-axis corresponds to the 21 different combinations of the A and B single-qubit gates.
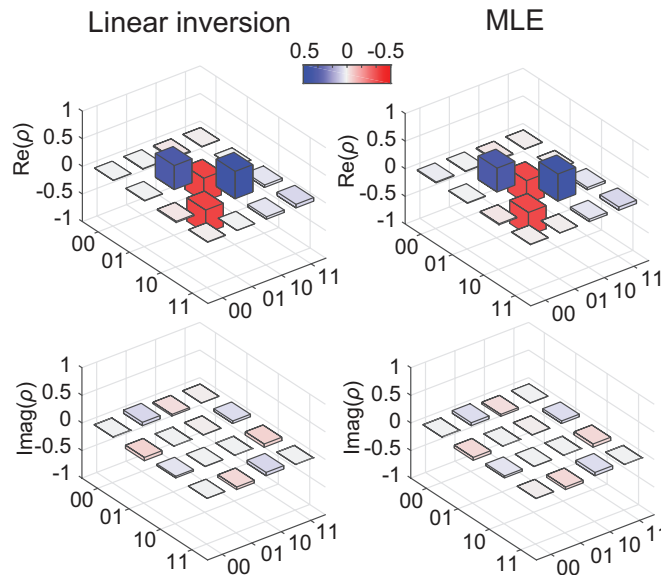
S3. STATE TOMOGRAPHY OF BELL STATES.

The density matrix of a two-qubit state can be expressed as $\rho = \sum_{i=1}^{16} c_i M_i$ where M_i are 16 linearly independent measurement operators. The coefficients c_i were calculated from the expectation values of the measurement operators either through linear inversion or a maximum likelihood estimation where the later ensures a physical density matrix that is Hermitian and positive semi-definite [3]. Fig. S4 shows a comparison of the density matrices for the state $\Psi^- = (|01\rangle - |10\rangle)/\sqrt{2}$ calculated using either linear inversion and MLE. The results are nearly identical indicating the estimated expectation values from the MLE are close to the measured expectation values in the experiment. For all measured states, the elements of the density matrix calculated with either linear inversion and MLE differ on average by ~ 0.005. The calculated density matrices for the four Bell states using MLE are:

$$\Psi^+ = \begin{pmatrix} 0.019 + 0i & 0.010 - 0.018i & -0.006 - 0.030i & -0.009 + 0.016i \\ 0.010 + 0.018i & 0.425 + 0i & 0.422 - 0.026i & -0.014 + 0.078i \\ -0.006 + 0.030i & 0.422 + 0.026i & 0.493 + 0i & -0.050 + 0.058i \\ -0.009 - 0.016i & -0.014 - 0.078i & -0.050 - 0.058i & 0.063 + 0i \end{pmatrix}, \tag{1}$$

$$\Psi^- = \begin{pmatrix} 0.016 + 0i & 0.009 + 0.052i & -0.016 - 0.035i & -0.008 + 0.005i \\ 0.009 - 0.052i & 0.429 + 0i & -0.420 - 0.007i & 0 + 0.050i \\ -0.016 + 0.035i & -0.420 + 0.007i & 0.495 + 0i & 0.040 - 0.062i \\ -0.008 - 0.005i & 0 - 0.050i & 0.040 + 0.062i & 0.060 + 0i \end{pmatrix}, \tag{2}$$

$$\Phi^+ = \begin{pmatrix} 0.501 + 0i & -0.024 + 0.023i & 0.002 + 0.021i & 0.370 + 0.013i \\ -0.024 - 0.023i & 0.019 + 0i & 0.003 - 0.003i & -0.03 - 0.028i \\ -0.002 - 0.021i & 0.003 + 0.003i & 0.013 + 0i & 0.017 + 0.019i \\ 0.370 - 0.013i & -0.031 + 0.028i & 0.017 - 0.019i & 0.467 + 0i \end{pmatrix}, \tag{3}$$

$$\Phi^- = \begin{pmatrix} 0.505 + 0i & 0.010 - 0.047i & -0.019 + 0.015i & -0.407 + 0.001i \\ 0.010 + 0.047i & 0.019 + 0i & -0.002 + 0.010i & -0.024 - 0.025i \\ -0.019 - 0.015i & -0.002 - 0.010i & 0.024 + 0i & 0.040 + 0.039i \\ -0.407 - 0.001i & -0.024 + 0.025i & 0.040 - 0.039i & 0.452 + 0i \end{pmatrix}, \tag{4}$$

Supplementary Fig. S4. **Comparison between the maximum likelihood estimation and linear inversion for the Bell state $\Psi^- = 1/\sqrt{2}(|01\rangle - |10\rangle)$.**

In quantum state tomography, the density matrix can be reconstructed by measuring the two-spin probabilities after applying 9 combinations of the prerotations I, X, Y. In the actual experiment, we also included the prerotation X^2 to help detect systematic errors leading to 16 combinations in total. Fig. S5 shows the real component of the estimated density matrices for the four Bell states and $\psi = (|10\rangle + |11\rangle)/\sqrt{2}$. These were calculated using either all prerotations or a subset of these prerotations, I, X, Y or X, Y, X^2. Using either X, Y, X^2 or I, X, Y, X^2 gives similar

results where the state fidelities and concurrences are $2-9\%$ and $4-11\%$ less than those calculated with I, X, Y. For the final estimate of the density matrices we use only the prerotations I, X, Y as I should give a better estimate for the expectation values than X^2 due to decoherence and small calibration errors in our system. We did not account for decoherence and other errors in the prerotation pulses, which likely causes us to underestimate the overlaps with the ideal Bell states. Future work will include incorporating the prerotation errors into the state tomography analysis.
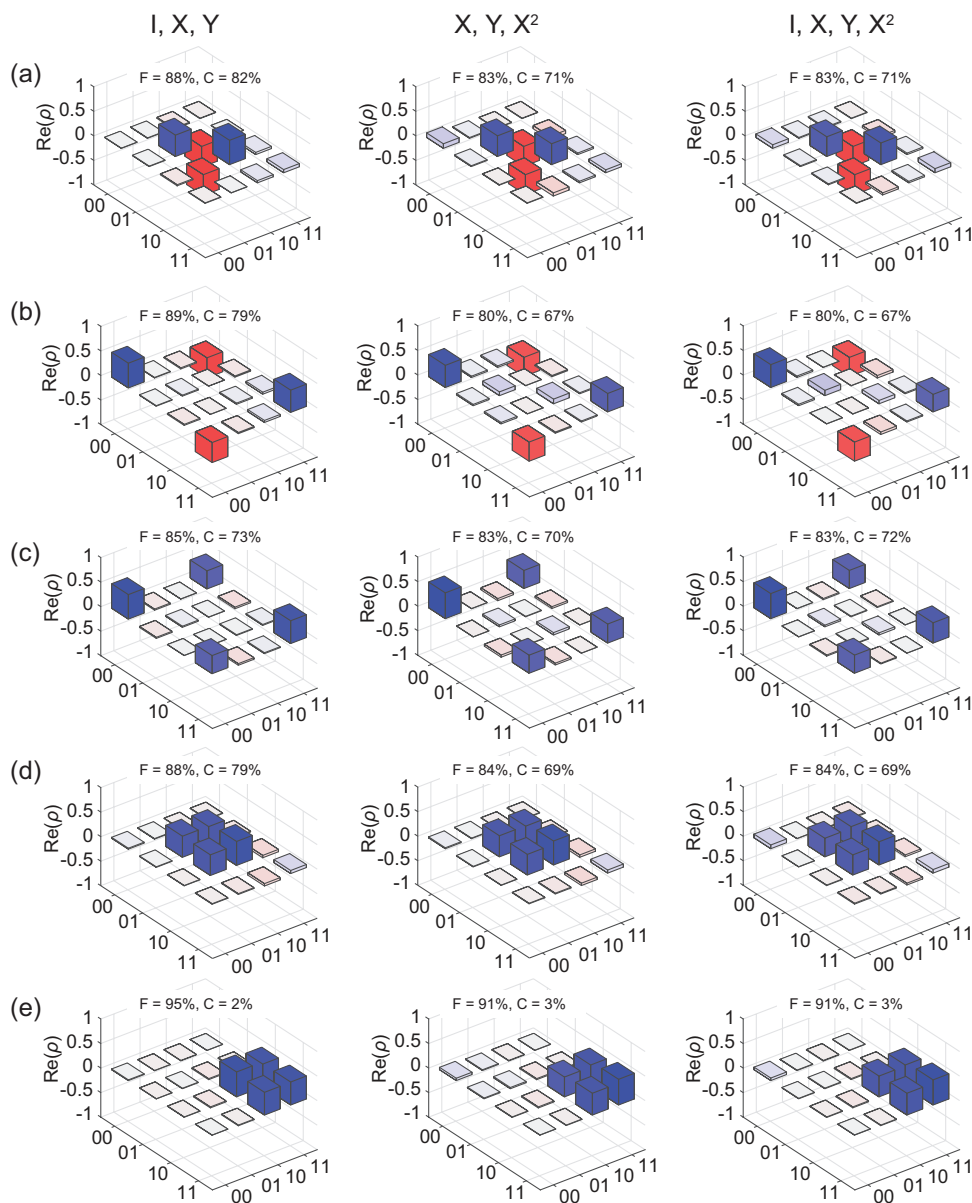
Supplementary Fig. S5. **Comparison between density matrices constructed using different prerotations.** The real component of the reconstructed density matrices using a maximum likelihood estimation for the four Bell states (a) $\Psi^+ = (|01\rangle + |10\rangle)/\sqrt{2}$, (b) $\Psi^- = (|01\rangle - |10\rangle)/\sqrt{2}$, (c) $\Phi^+ = (|00\rangle + |11\rangle)/\sqrt{2}$, (d) $\Phi^- = (|00\rangle - |11\rangle)/\sqrt{2}$, and (e) $\psi = (|10\rangle + |11\rangle)/\sqrt{2}$. Here, the columns label whether the I, X, Y or X, Y, X^2 or I, X, Y, X^2 prerotations were used to calculate the expectation values in the estimation of the density matrices.

[1] S. Freer, S. Simmons, A. Laucht, J. T. Muhonen, J. P. Dehollain, R. Kalra, F. A. Mohiyaddin, F. E. Hudson, K. M. Itoh, J. C. McCallum, D. N. Jamieson, A. S. Dzurak, and A. Morello, "A single-atom quantum memory in silicon," Quantum Science and Technology **2**, 015009 (2017).

[2] L. M. K. Vandersypen and I. L. Chuang, "NMR techniques for quantum control and computation," Rev. Mod. Phys. **76**, 1037–1069 (2005).

[3] D. F. V. James, P. G. Kwiat, W. J. Munro, and A. G. White, "Measurement of qubits," Phys. Rev. A **64**, 052312 (2001).